

Automated Extraction of Building Outlines From Airborne Laser Scanning Point Clouds

Bisheng Yang, Wexue Xu, and Zhen Dong

Abstract—Automatic extraction of building outlines from airborne laser scanning (ALS) point clouds has been an active topic in the field of photogrammetry, remote sensing, and computer vision. In this letter, a marked point process method is implemented to extract building outlines from ALS point clouds. First, the Gibbs energy model of building objects is defined to describe the building points. Second, the defined Gibbs energy model is sampled within the framework of reversible-jump Markov chain Monte Carlo and optimized to find an optimal energy configuration by simulated annealing. Finally, the detected building objects are refined to eliminate false detections, and the outlines of buildings are derived from the detected building objects by morphological operators. The standard data set provided by ISPRS is used to verify the validity of the proposed method. The method extracted building objects from the standard data sets with an average completeness of 87.3% and correctness of 91.57% at the pixel level, and an average completeness of 77.6% (97.3%) and correctness of 98.1% (97.9%) at the object (object > 50 m²) level.

Index Terms—Airborne laser scanning (ALS), building outlines, marked point processes.

I. INTRODUCTION

AIRBORNE laser scanning (ALS) point clouds are widely used in roof reconstruction, digital elevation modeling (DEM) generations, building outline detection, and tree crown delineation. Numerous studies have investigated the extraction of building outlines and the reconstruction of roofs [1]–[4]. One solution is to first filter the ground points and then label the non-ground points according to operators, such as region growing [5] and plane detection [6]. The second solution is to classify either full-wave data or multi-echo ALS points into roads, building roofs, and trees [7], [8]. The classification results mainly depend on the selection of classification methods and decision-making principles (e.g., Bayesian). Another solution is to register ALS point clouds and auxiliary data (e.g., imagery, vector map) to extract buildings [9]–[11]. Based on the extracted building points, the corresponding building outlines can thus be derived. As far as the first category of solutions is concerned, the extraction of buildings depends heavily on the quality of ground point filtering. On the other

Manuscript received January 17, 2013; revised March 22, 2013 and April 4, 2013; accepted April 16, 2013. Date of publication June 26, 2013; date of current version October 10, 2013. This work was supported by the National Basic Research Program of China under Grant 2012CB725301 and the National Science Foundation of China project under Grant 41071268.

The authors are with the State Key Laboratory of Information Engineering in Surveying, Mapping, and Remote Sensing, Wuhan University, Wuhan 430079, China (e-mail: bshyang@whu.edu.cn).

Color versions of one or more of the figures in this paper are available online at <http://ieeexplore.ieee.org>.

Digital Object Identifier 10.1109/LGRS.2013.2258887

hand, auxiliary data (e.g., imagery) are not always available, and the registration between them is still a nontrivial issue.

Stochastic geometry methods, such as Markov random field (MRF), have achieved promising effects in road extraction and object recognition [12], [13]. Nevertheless, MRF is heavily affected by noise and easily falls into local minimum values. Marked point process is an object-oriented stochastic geometry method. It solves the above problems well and has been widely used to extract objects from high-resolution imageries. Ortner and Tournaire presented a method based on marked point processes to extract building footprints from high-resolution digital elevation models [14], [15]. Ortner constructed a building energy model with multiple parameters that have to be tuned simultaneously, which is computationally intensive. In Tournaire's method, the data coherence energy term depends on the value of the mean gradient of each edge of the building footprints. The method is weak in extracting the building footprints of dense building areas. Tournaire proposed a marked point process-based approach to detect the dashed lines of road markings from high-resolution aerial images [13].

We implemented a marked point process method for extracting building outlines from ALS point clouds. Our main contributions are as follows:

- an energy model of building objects is modeled to fit the building points;
- fewer parameters are tuned, resulting in light computing burden; and
- building objects are directly extracted from ALS point clouds without converting the latter into imagery.

We propose a framework of marked point processes for extracting building outlines from ALS point clouds. The framework consists of three key steps. First, the Gibbs energy model of building objects is defined to best fit the points of buildings. Second, the reversible-jump Markov chain Monte Carlo (RJMCMC), coupled with simulated annealing, is used to find a maximum a posteriori estimate of the number, locations, and sizes of building objects described by the Gibbs energy model. Finally, the points of each Gibbs energy model are refined to eliminate false building points and then used to derive the corresponding building outlines.

II. MARKED POINT PROCESSES FOR DETECTING BUILDING OBJECTS

In statistics and probability theory, a point process is a type of random process in which any one realization consists of a set of isolated points either in time or geographical space, or

in even more general spaces [16]. A marked point process $S = K \times M$ is a point process in object space K , where each point is associated with a mark from a bounded set M . Marked point processes have been successfully used in extracting objects (e.g., road markings, buildings) from high-resolution imagery [12]–[15]. In object space K , the configurations of different types of objects should be modeled. According to the framework of marked point processes, each configuration of objects is associated with energy. Hence, the energy of building objects should be modeled for the purpose of extraction from ALS point clouds.

Building objects in ALS point clouds can be regarded as a Poisson process [17]. Let L be a set and d be a metric on L . Let $v(\bullet)$ be a Borel measure on a complete separable metric space (L, d) such that $v(L) > 0$ and $v(B) < \infty$ for all bounded Borel sets B . A point process X on L is a Poisson process with intensity measure $v(\bullet)$ if

- 1) $N(B)$ is Poisson distributed with mean $v(B)$ for every bounded Borel set $B \subseteq L$; and
- 2) for any k disjoint bounded Borel sets B_1, B_2, \dots, B_k , the random variables $N(B_1), N(B_2), \dots, N(B_k)$ are independent [18].

Let us consider a homogeneous Poisson process with intensity measure $v(\bullet)$, and let $h(\bullet)$ be a nonnegative function on the configuration space Λ . Then, the measure $\mu(\bullet)$ having density $h(\bullet)$ with respect to $v(\bullet)$ is defined as [19]: $m(B) = \int_B h(x)v(dx)$. The density $h(\bullet)$ can be defined in two ways: in a Bayesian framework, which requires having a model of heights in the whole area, or through the Gibbs energy [15]. We choose the second form because it is usually difficult to build a height model that is valid for the whole area of interest. Thus, the density $h(\bullet)$ of marked point processes X_t is written as [19]

$$h(x) = \frac{1}{Z} \exp(-U(x)) \quad (1)$$

where Z is a normalizing constant, and $Z = \sum_{x \in \Omega} \exp(-U(x))$. Moreover, the Gibbs energy $U(\bullet)$ can be expressed as a weighted sum of a data coherence term energy, which qualifies the quality of the objects (external energy) and a prior constraint energy measuring the spatial quality of the collection of objects (prior or internal energy). The Gibbs energy is written as

$$U(x) = U_d(x) + U_p(x); \quad x \in \Lambda_k. \quad (2)$$

A. Gibbs Energy Model of Buildings

Objects for Modeling Buildings: To define the objects associated with buildings and the corresponding marks, we build the prior terms and data associated with buildings, resulting in the global energy of the model. We define the base object associated with buildings as cuboid and the corresponding marks in each cuboid as follows:

- the orientation $q \in [0, \pi]$ is the orientation of building outlines in the plane of XoY ;
- the height $h \in [h_{\min}, h_{\max}]$ is the height of buildings;
- the length $l \in [l_{\min}, l_{\max}]$ is the length of buildings;
- the width $w \in [w_{\min}, w_{\max}]$ is the width of buildings.

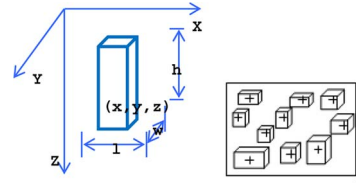


Fig. 1. Base object and marked point processes.

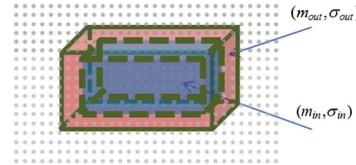


Fig. 2. Data coherence measurement between a building object and its surrounding points.

The cuboids associated with buildings consist of the marked point processes of cuboids (Fig. 1). The associated set spaces are described as

$$S_{cuboid} = [l_{\min}, l_{\max}] \times [w_{\min}, w_{\max}] \times [h_{\min}, h_{\max}] \times [0, \pi]. \quad (3)$$

In light of the framework of marked point processes, the data coherence term and the prior constraint term associated with buildings should be modeled for the global energy of building objects.

Data Coherence Term of Buildings: The data coherence term $U_d(x)$ of buildings, which accumulates the local energy associated with each building x_i of the configuration x , is written as

$$U_d(x) = \sum_i U_d(x_i) \quad (4)$$

where $U_d(x_i)$ is a measure of the coherence of the building x_i with respect to its surrounding ALS point clouds. This measurement must satisfy both the independence of each building and the locally negative energy of well-fitted buildings [19]. The inside region of one building is the envelope region of the building outline. The boundary of the inside region is expanded outside a certain width (e.g., 1 m) to form an area that is defined as the outside region of one building (Fig. 2). The blue and red dotted parts in Fig. 2 indicate the inside and outside regions of the building, respectively. Hence, $U_d(x_i)$ is written as

$$U_d(x_i) = \begin{cases} 1 - \frac{d_m}{d_0} & d_m < d_0 \\ \frac{d_0}{d_m} - 1 & d_m \geq d_0 \end{cases}$$

$$d_m = \sqrt{\frac{(m_{in} - m_{out})^2 * (n_1 + n_2 - 2)}{\delta_{in}^2 * (n_1 - 1) + \delta_{out}^2 * (n_2 - 1)}} \quad (5)$$

where d_m is the Mahalanobis distance between the inside and the outside region of one building; m_{in} and m_{out} refer to the mean elevation of the ALS points in the inside and the outside region of the building, respectively; δ_{in} and δ_{out} are the standard deviations of the elevations of the ALS points in the inside and the outside region of the building, respectively; and n_1 and n_2 refer to the number of ALS points in the inside and the outside region of the building, respectively.

Mahalanobis distance is better than Bhattacharyya distance, which may bring considerable errors when its first and second terms are in the same order [20]. The threshold d_0 allows us to select the attractive objects and tune the sensitivity of the data fitting.

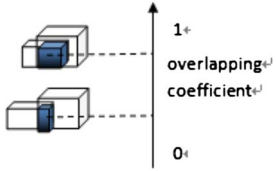


Fig. 3. Measurement of overlapping objects.

Prior Constraint Term of Buildings: The prior constraint term $U_p(x)$ of building objects introduces prior knowledge on buildings by taking into account the pairwise interactions between buildings and the gradient of building outlines. To avoid over-detection of buildings, a penalty term between two overlapping buildings is measured by (Fig. 3)

$$U_a(x) = \sum_{i,j=1, i < j}^n \frac{V(x_i \cap x_j)}{\min(V_{xi}, V_{xj})} \quad (6)$$

where x_i and x_j are building objects in the configuration of x ; V_{xi} and V_{xj} are the volumes of x_i and x_j , respectively; and $V(x_i \cap x_j)$ is the volume of the overlapping part of x_i and x_j .

To avoid extreme closeness between objects, an infinite energy is assigned to pairs of too-close objects. Distance threshold h is specified to control the minimum distance between cuboids. We set h to 3 m for extracting buildings.

$$U_s(x) = \begin{cases} +\infty & (x_i, x_j) \in x, d(x_i, x_j) < h \\ 0 & \text{otherwise} \end{cases} \quad (7)$$

where x_i and x_j are building objects in the configuration of x ; and $d(x_i, x_j)$ is the distance between the central points of x_i and x_j . On the other hand, the gradient constraint of building outlines is integrated into the prior knowledge on buildings. Supposing that the gradient of the cuboid edge is less than a specified threshold, the cuboid will be assigned a penalty; this is written as

$$U_g(x) = \sum_{i=0}^n 0.25 * n_{xi} \quad (8)$$

where n_{xi} is the number of edges having a gradient less than a specified threshold. The threshold of the gradient is specified as 1.5, indicating that the minimum height of buildings should be more than 1.5 m.

Besides, the gradient constraint of building outlines, the filling percentage of points in cuboids (f_i), which is the number of points in each cuboid divided by the area of the cuboid outline, is also taken as a prior constraint. The prior term associated with the filling factor of each cuboid is calculated by

$$U_f(x_i) = \begin{cases} \frac{f_{threshold} - f_i}{1 - f_{threshold}} & \text{if } f_i \geq f_{threshold} \quad f_{min} = 0.5 \\ \frac{f_{threshold} - f_i}{f_{threshold} - f_{min}} & \text{if } f_{min} < f_i < f_{threshold} \quad f_{threshold} = 0.7 \\ +\infty & \text{if } f_i \leq f_{min}. \end{cases} \quad (9)$$

Finally, the prior energy associated with building objects is written as

$$U_p(x) = U_a(x) + U_s(x) + U_g(x) + U_f(x). \quad (10)$$

Hence, the global energy of building objects for a given marked point process is written as

$$U(x) = U_d(x) + U_p(x). \quad (11)$$

B. Finding the Optimal Energy With RJMCMC

The global optimal solution of the global energy $U(x)$ will be sampled using RJMCMC coupled with simulated annealing [13]. Green proposed an RJMCMC method, which is a special Metropolis-Hastings method, that can include reversible jumps between different subspaces [21]. RJMCMC is useful for simulating probability distributions that are a mixture of distributions having support for different dimensions [22]. In the framework of RJMCMC, birth and death kernels are sufficient to guarantee the convergence of the Markov chain.

The steps of the Metropolis–Hastings–Green algorithm are as follows:

Let $q(y|x)$ be an arbitrary proposition kernel for a given state space X_i :

- 1) Randomly choose a proposition kernel, and then generate a new state space $Y \sim q(y|X_i)$.
- 2) Compute Green's ratio $r(X_i, Y)$: $r(X_i, Y) = \min\{(f(Y)/f(X_i))(q(X_i|Y)/q(Y|X_i)), 1\}$,

where $f(X_i)$ and $f(Y)$ denote the global energy of all buildings in state space X_i and state space Y , respectively; and $q(X_i|Y)$ and $q(Y|X_i)$ denote the changing probability from state space X_i to state space Y and from state space Y to state space X_i .

- 3) Set $X_{i+1} = \begin{cases} Y & \text{with probability } r \\ X_i & \text{with probability } 1 - r \end{cases}$.

In the optimization process, we use seven different proposition kernels, namely, birth, death, translation, rotation, dilation, split, and merge, to guarantee the irreducibility and the reversibility of the Markov chain. The effectiveness of the seven proposition kernels has been proven in [13]. For each proposition kernel used in the proposed method, the Green's ratio computation can be found in references [16], [19], [21].

Simulated Annealing: Simulated annealing ensures convergence to the global optimum regardless of the initial configuration [19]. Generally, a geometric decreasing solution is selected to decrease the temperature [13], and this is written as

$$T_t = T_0 * \alpha^t \quad (12)$$

where T_0 is the initial temperature, α is the decreasing coefficient and close to 1, and t is the time of decreasing temperature.

In our experiment, we set T_0 to 1 because we found that the energy variation of $U(x)$ becomes disordered when the temperature decreases from 1000 to 1. The decreasing coefficient of α is set to 0.9995.

To accelerate the convergence speed of $U(x)$, we define the following schemes:

- The energy of each building object is recorded and tracked during each iteration. Supposing that the data coherence energy of one building object remains stable for consecutive m iterations ($m > 10$), the building object will be removed from the Markov chain and maintained as an output.
- Supposing that the total energy of the objects in the Markov chain remains stable for consecutive k iterations ($k > 3000$), the configuration of energy $U(x)$ is regarded as convergent, and the whole process is terminated.

Once the Markov chain is convergent, each object in the chain is regarded as a building object that is described by a cuboid with an orientation.

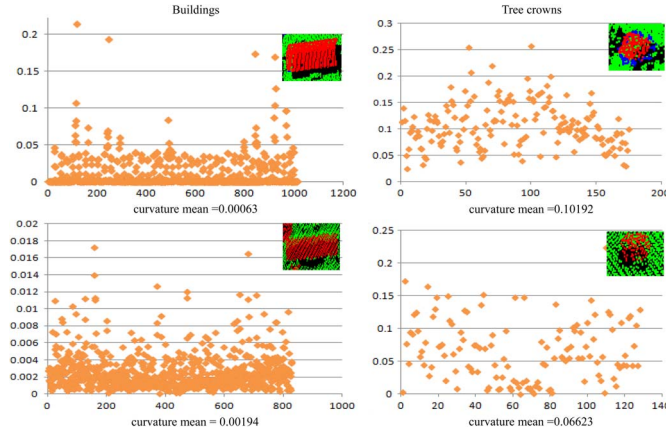


Fig. 4. Statistical comparison of the curvature distribution between buildings and tree crowns.

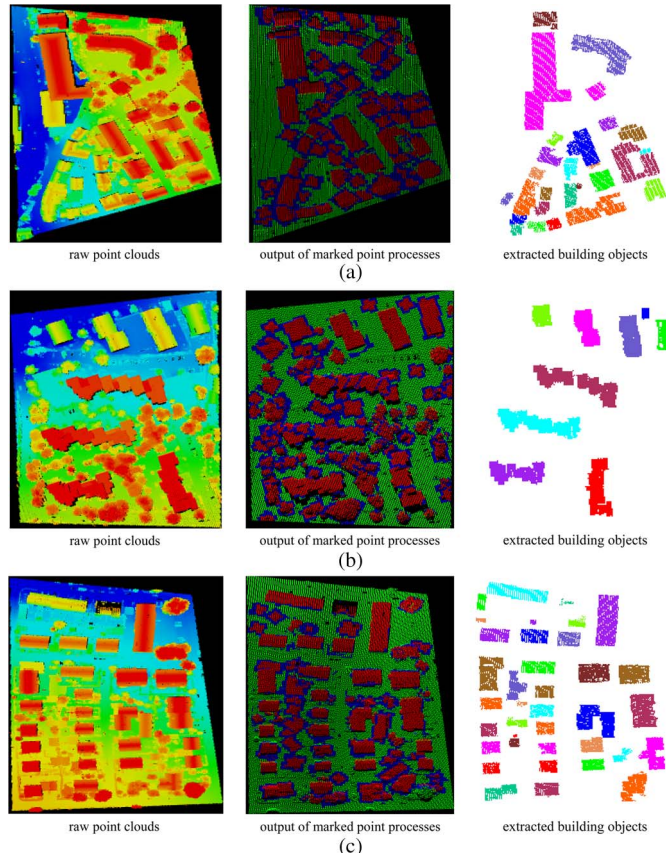


Fig. 5. Building outline extraction in three test areas. (a) area 1; (b) area 2; (c) area 3.

III. REFINING THE DETECTED BUILDING OBJECTS

Because the energy model of buildings only considers the coherence of the inside region and the difference between the inside and the outside region, a lot of objects (e.g., dense trees) are detected as building objects. To eliminate misclassified objects, the curvatures of the points in each detected cuboid are calculated. Fig. 4 illustrates a statistical comparison of the curvature distribution between building objects and tree crowns (red points), showing that the curvatures of tree crowns are several times larger than those of building objects because tree



Fig. 6. Evaluation on a per-object level from the point of view of the reference data.

crowns and building roofs display different shapes. Hence, a smaller value (e.g., 0.003) can be specified to remove tree crowns from the detected cuboids. Finally, the method presented in [23] is used to trace the outlines of building objects from the refined point clouds.

IV. EXPERIMENT AND ANALYSIS

The proposed model was tested with the LiDAR data set of Vaihingen, Germany [24], in the context of the “ISPRS Test Project on Urban Classification and 3-D Building Reconstruction.” Three areas of the data set were selected as the standard test data sets.

A. Building Detection Results and Discussion

Fig. 5 illustrates the detected buildings and the corresponding outlines of the three areas. Compared with the refined building points, the output of the proposed marked point process method was found to have improved greatly by refining the point clouds in each detected cuboid according to the curvature analysis and the cuboid sizes [Fig. 5(b) and (c)]. The comprehensive evaluation and comparison of the detected outlines of buildings were performed by the ISPRS Workgroup III/4 based on the method described in [25]. Fig. 6 illustrates the results on a per-object level from the point of view of the reference data.

The correctness and completeness of the extraction of building objects was evaluated based on the method described by the ISPRS Workgroup III/4 in [25] (Table I). As can be seen from Table I, the proposed method extracted building objects with an average completeness of 87.3% and correctness of 91.57% at the pixel level, and with an average completeness of 77.6% (97.3%) and correctness of 98.1% (97.9%) at the

TABLE I
CORRECTNESS AND COMPLETENESS OF
BUILDING OBJECTS EXTRACTION

| Evaluation method | | Area 1 | Area 2 | Area 3 |
|-------------------|------------------|--------|--------|--------|
| Per area | Completeness [%] | 87.9 | 88.8 | 85.2 |
| | Correctness [%] | 91.2 | 94.0 | 89.5 |
| Per object | Completeness [%] | 81.1 | 78.6 | 73.2 |
| | Correctness [%] | 96.8 | 100 | 97.6 |
| >50m ² | Completeness [%] | 100 | 100 | 92.1 |
| | Correctness [%] | 96.6 | 100 | 97.2 |
| RMSE [m] | | 0.9 | 0.8 | 0.8 |

object (object > 50 m²) level. A full comparison between the proposed method (WHU_Y) and 10 other methods can be found on the ISPRS website [26]. The comparison shows that the proposed method extracted buildings with good accuracy.

Compared with methods based on traditional marked point processes [13]–[15], [19], the Gibbs energy model proposed herein for building objects has only one parameter (d_0) to be tuned manually, thus easing the burden of tuning parameters. For the three areas, the parameter d_0 is specified as 1.2. The other parameters (e.g., the sizes of cuboids, the gradients of buildings) for calculating the energy of building objects can be specified within a loose range. On the other hand, the ALS point clouds are directly processed to extract building objects, overcoming the information loss due to raw points being converted into raster imagery. The average computation times per building of the test data sets are about 3.6, 2.3, and 2.2 min, respectively.

V. CONCLUSION

The proposed method was tested using standard test data sets provided by the ISPRS, and the results indicate that:

- the constructed Gibbs energy model of building objects is effective and valid for modeling buildings in ALS point clouds;
- the beneficial attempt to extract meaningful objects from ALS point clouds based on marked point processes provides a functional and effective solution for directly extracting objects from ALS point clouds; and
- the entire process is automatic and requires little human aid, which is a promising solution for ALS point clouds processing.

ACKNOWLEDGMENT

The Vaihingen data set was provided by the German Society for Photogrammetry, Remote Sensing and Geoinformation (DGPF). Special thanks go to Dr. Markus Gerke of the ITC, the Netherlands, for evaluating the building outlines extracted with the proposed method.

REFERENCES

- [1] N. Haala and C. Brenner, "Extraction of buildings and trees in urban environments," *ISPRS J. Photogramm. Remote Sens.*, vol. 54, no. 2/3, pp. 130–137, Jul. 1999.
- [2] L. Sahar, S. Muthukumar, and S. P. French, "Using aerial imagery and GIS in automated building footprint extraction and shape recognition for earthquake risk assessment of urban inventories," *IEEE Trans. Geosci. Remote Sens.*, vol. 48, no. 9, pp. 3511–3520, Sep. 2010.
- [3] K. Zhang, J. Yan, and S. C. Chen, "Automatic construction of building footprints from airborne LiDAR data," *IEEE Trans. Geosci. Remote Sens.*, vol. 44, no. 9, pp. 2523–2533, Sep. 2006.
- [4] K. Kim and J. Shan, "Building roof modeling from airborne laser scanning data based on level set approach," *ISPRS J. Photogramm. Remote Sens.*, vol. 66, no. 4, pp. 484–497, Jul. 2011.
- [5] S. Filin, "Surface clustering from airborne laser scanning data," *Int. Archives Photogramm. Remote Sens. Spatial Inf. Sci.*, vol. 34, no. 3A, pp. 117–124, 2002.
- [6] F. Rottensteiner, J. Trinder, S. Clode, and K. Kubik, "Detecting buildings and roof segments by combining LiDAR data and multispectral images," in *Proc. IVCNZ*, Palmerston North, New Zealand, 2003, pp. 60–65.
- [7] C. Alexandra, K. Tansey, J. Kaduka, D. Holland, and N. J. Tatea, "An approach to classification of airborne laser scanning point cloud data in an urban environment," *Int. J. Remote Sens.*, vol. 32, no. 24, pp. 9151–9169, Dec. 2011.
- [8] K. Khoshelham, C. Nardinocchi, E. Frontoni, A. Mancini, and P. Zingaretti, "Performance evaluation of automated approaches to building detection in multi-source aerial data," *ISPRS J. Photogramm. Remote Sens.*, vol. 65, no. 1, pp. 123–133, Jan. 2010.
- [9] G. Vosselman and S. Dilkman, "3D building model reconstruction from point clouds and ground plan," *Int. Archives Photogramm. Remote Sens. Spatial Inf. Sci.*, vol. XXXIV-3/W4, pp. 37–43, Oct. 2001.
- [10] G. Sohn and I. Dowman, "Data fusion of high-resolution satellite imagery and LiDAR data for automatic building extraction," *ISPRS J. Photogramm. Remote Sens.*, vol. 62, no. 1, pp. 43–63, May 2007.
- [11] L. Cheng, J. Y. Gong, M. C. Li, and Y. X. Liu, "3D building model reconstruction from multi-view aerial images and LiDAR data," *Photogramm. Eng. Remote Sens.*, vol. 77, no. 2, pp. 125–139, Feb. 2011.
- [12] G. Perrin, X. Descombes, and J. Zerubia, "Point processes in forestry: An application to tree crown detection," INRIA, Cedex, France, Research Rep. 5544, 2005.
- [13] O. Tournaire and N. Paparoditis, "A geometric stochastic approach based on marked point processes for road mark detection from high resolution aerial images," *ISPRS J. Photogramm. Remote Sens.*, vol. 64, no. 6, pp. 621–631, Nov. 2009.
- [14] M. Ortner, X. Descombes, and J. Zerubia, "Building outline extraction from digital elevation models using marked point processes," *Int. J. Comput. Vis.*, vol. 72, no. 2, pp. 107–132, Apr. 2007.
- [15] O. Tournaire, M. Bredif, D. Boldo, and M. Durupt, "An efficient stochastic approach for building footprint extraction from digital elevation models," *ISPRS J. Photogramm. Remote Sens.*, vol. 65, no. 4, pp. 317–327, Jul. 2010.
- [16] D. L. Snyder, *Random Point Processes*. New York, NY, USA: Wiley, 1975.
- [17] R. Durrett, *Probability: Theory and Examples*, 4th ed. Cambridge, U.K.: Cambridge Univ. Press, 2010.
- [18] M. Van Lieshout, *Markov Point Processes and Their Applications*. London, U.K.: Imperial College Press, 2000.
- [19] F. Lafarge, G. Gimelfarb, and X. Descombes, "Geometric feature extraction by a multi-marked point process," *IEEE Trans. Pattern Anal. Mach. Intell.*, vol. 32, no. 9, pp. 1597–1609, Sep. 2010.
- [20] G. R. Xuan, P. Q. Chai, and M. H. Wu, "Bhattacharyya distance feature selection," in *Proc. 13th Int. Conf. Pattern Recognit.*, 1996, vol. 2, pp. 195–199.
- [21] P. Green, "Reversible jump markov chains monte carlo computation and bayesian model determination," *Biometrika*, vol. 82, no. 4, pp. 711–732, Dec. 1995.
- [22] C. J. Geyer, The Metropolis-Hastings-Green algorithm 2003, mimeo.
- [23] B. S. Yang, Z. Wei, Q. Q. Li, and J. Li, "Semiautomated building facade footprint extraction from mobile LiDAR point clouds," *IEEE Geosci. Remote Sens. Lett.*, vol. 10, no. 4, pp. 766–770, Jul. 2013.
- [24] M. Cramer, "The DGPF-test on digital airborne camera evaluation—Overview and test design," *Photogrammetrie-Fernerkundung-Geoinformation*, vol. 2010, no. 2, pp. 73–82, May 2010.
- [25] M. Rutzinger, F. Rottensteiner, and N. Pfeifer, "A comparison of evaluation techniques for building extraction from airborne laser scanning," *IEEE Sel. Topics Applied Earth Observ. Remote Sens.*, vol. 2, no. 1, pp. 11–20, Mar. 2009.
- [26] Results of 'ISPRS Test Project on Urban Classification and 3D Building Reconstruction', (accessed March 15, 2013). [Online]. Available: <http://www2.isprs.org/commissions/comm3/wg4/results.html>